

**\*\*Volume Title\*\***  
**ASP Conference Series, Vol. \*\*Volume Number\*\***  
**\*\*Author\*\***  
 © **\*\*Copyright Year\*\*** *Astronomical Society of the Pacific*

## Global-scale Simulations of Stellar Convection and their Observational Predictions

Benjamin P. Brown<sup>1,2</sup>

<sup>1</sup>*Department of Astronomy,  
 University of Wisconsin, 475 Charter Street, Madison, WI 53706-1582*

<sup>2</sup>*Center for Magnetic Self Organization (CMSO)  
 in Laboratory and Astrophysical Plasmas,  
 University of Wisconsin, 1150 University Avenue, Madison, WI 53706*

**Abstract.** Stars on the lower main sequence (F-type through M-type) have substantial convective envelopes beneath their stellar photospheres. Convection in these regions can couple with rotation to build global-scale structures that may be observable by interferometers that can resolve stellar disks. Here I discuss predictions emerging from 3D MHD simulations for solar-type stars with the anelastic spherical harmonic (ASH) code and how these predictions may be observationally tested. The zonal flow of differential rotation is likely the most easily observable signature of dynamics occurring deep within the stellar interior. Generally, we find that rapidly rotating suns have a strong solar-like differential rotation with a prograde equator and retrograde poles while slowly spinning suns may have anti-solar rotation profiles with fast poles and slow equators. The thermal wind balance accompanying the differential rotation may lead to hot and bright poles in the rapid rotators and cooler, darker poles in slow rotators. The convection and differential rotation build global-scale magnetic structures in the bulk of the convection zone, and these wreaths of magnetism may be observable near the stellar surfaces.

### 1. Introduction

When stars like our Sun are young, they rotate rapidly and have strong magnetic fields at their surfaces. Magnetic activity is a nearly ubiquitous feature of F- to M-type stars on the lower main sequence, all of which have convective envelopes just below their photospheres. Younger and more rapidly rotating stars are generally more active and follow the “rotation-activity” relationship (see e.g., Pizzolato et al. 2003). Stellar magnetic fields are thought to arise from dynamo processes occurring in these stellar convection zones, where turbulent plasma motions couple with rotation to build global-scale magnetic fields. At present, stellar dynamo theory does not explain the observed correlation between rotation and magnetic activity. Likewise, our own Sun’s eleven year magnetic activity and sunspot cycles remains a puzzling mystery: despite intense study, solar dynamo models are at present unable to reliably predict even large-scale features of the solar cycle.

The nature of solar and stellar dynamos, and the origin of solar and stellar magnetic fields, remains one of the most important unsolved problems in stellar astrophysics. In modern times, the tremendous growth of computational resources, coupled with de-

tailed pictures of flows and structure within the solar interior from helioseismology, has led to an explosion of dynamo modeling efforts, ranging from sophisticated 2D mean-field models to fully 3D simulations that can capture the non-linear dynamics of solar convection self-consistently. Indeed it is now possible to model global-scale convection and dynamo action in the Sun with some fidelity (e.g., Brun & Toomre 2002; Brun et al. 2004; Browning et al. 2006; Miesch et al. 2006, 2008; Miesch & Toomre 2009; Ghizaru et al. 2010; Racine et al. 2011) and those efforts are being extended to other solar-type stars. The progress in solar simulations was helped tremendously by detailed observations of the Sun which constrained and challenged the simulations. Detailed observations of other stars will likewise be necessary for further progress in a general understanding of stellar convection and dynamo action, which will itself aid our understanding of the solar interior.

Here I will discuss recent global-scale 3D magnetohydrodynamic (MHD) simulations of stellar convection with the anelastic spherical harmonic (ASH) code (Clune et al. 1999; Brun et al. 2004). This code has been used to simulate solar convection and reproduces the observed solar differential rotation profile relatively well (e.g., Miesch et al. 2006, 2008). Building on this success, we have conducted a series of simulations for solar-type stars rotating more rapidly than the Sun (Brown et al. 2008) and have explored the dynamo-generated magnetic fields in several of these cases (Brown et al. 2010, 2011; Brown 2011). These simulations are beginning to make specific observational predictions which optical interferometry may be able to test, and here we will begin laying out what those questions are and how they may be answered.

## 2. Simulating stellar convection

One path towards understanding stellar convection is to conduct simulations of the plasma motions occurring within the stellar interior. Stellar convection spans a vast range of spatial and temporal scales, which lie well beyond the grasp of direct numerical simulation even on the largest modern supercomputers. Consequently, models of stellar convection and dynamo action must make various tradeoffs, either building up from the smallest diffusive scales or building down from the global-scales. The later global-scale simulations will be our focus here, and it is these simulations that can self-consistently capture the interactions between convection and rotation in a stratified atmosphere to drive global-scale flows of differential rotation. These simulations remain distant from stellar parameters, and a sense of this gap is given in Brown (2011).

## 3. Global-scale signatures of convection

The patterns of convection arising in simulations of solar-type stars at a variety of rotation rates are shown in Figure 1. These simulations span from 0.5 to 10  $\Omega_{\odot}$ , with  $\Omega_{\odot}$  the current solar rotation rate. These are labeled G0.5 through G10 respectively. When the rotation rate is slow relative to convective motions (equivalently, the Rossby number is large) then rotational constraints are weak and convective patterns are very similar in both polar and equatorial regions. This is evident in case G0.5 (Fig. 1a). As the rotation rate increases (Rossby number decreases), significant differences between the equator and pole emerge. Convection near the equator aligns with the rotation axis, forming “banana-cells” of convection. Near the poles the convection is more isotropic,

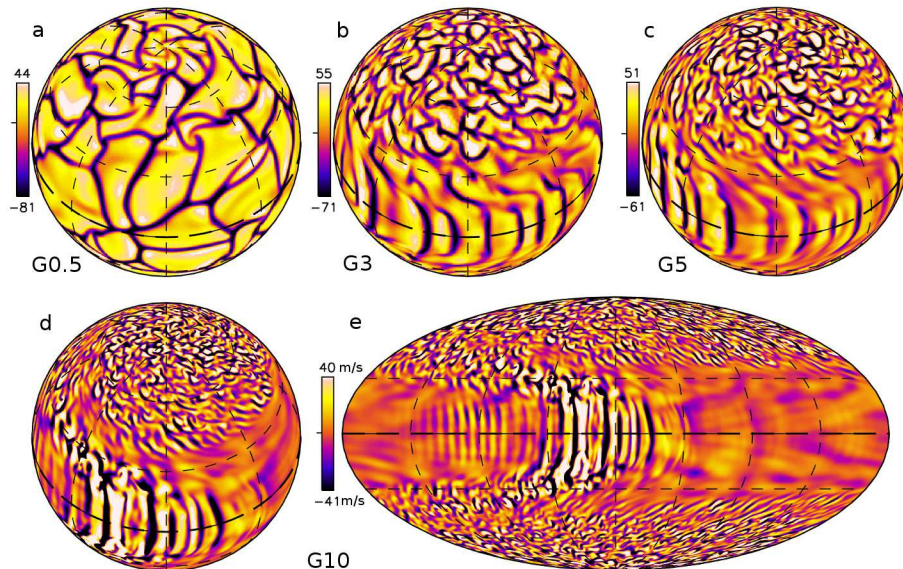


Figure 1. Patterns of convection in solar-type stars. Shown are radial velocity patterns near the stellar surface for stars rotating at (a)  $0.5 \Omega_{\odot}$ , (b)  $3 \Omega_{\odot}$ , (c)  $5 \Omega_{\odot}$ , and (d)  $10 \Omega_{\odot}$ . The broad, slow upflows are shown in light tones while the narrow, fast downflows are shown in dark tones. The north pole is visible and the equator is denoted by a dashed line. Clear differences are apparent in the polar and equatorial regions, and these become more pronounced as the rotation rate increases. At the highest rotation rates, convection near the equator can become confined to narrow bands in longitude. To emphasize this in case G10 we show the whole sphere from (d) in a Mollweide view in (e), with equator at middle and poles at top and bottom. These active nests of convection retain their identity for many thousands of days and propagate at speeds distinct from the stellar rotation rate (Brown et al. 2008).

with narrow downflow lanes surrounding broader upflows (e.g., case G5 in Fig. 1c). As the rotation rate is increased the horizontal scale of individual convective cells becomes smaller. Individual global-scale convective cells will likely be nearly impossible to detect on main-sequence solar-type stars; indeed their detection has eluded helioseismic detection in the solar interior for many years.

At the highest rotation rates however, surprising patterns of localized convection emerge, and these self-organized structures may create strong observational signatures. Here flows near the equator may be confined to one or two active ranges of longitude, with quiescent streaming flow in between. One such active nest of convection is shown in case G10 in Figure 1d, with Figure 1e showing the entire near-surface layer in a global Mollweide view. These active nests of convection are very long lived structures that persist for thousands of days (many hundreds of convective turnover times or rotation periods). They move at their own angular velocity, distinct from either the stellar rotation rate or the differential rotation in which they are embedded and at times may cover a substantial fraction of the stellar disk. These structures have been found in hydrodynamic simulations (Brown et al. 2008) and in some situations they survive in the presence of magnetism. In these cases they can act to concentrate surface magnetism

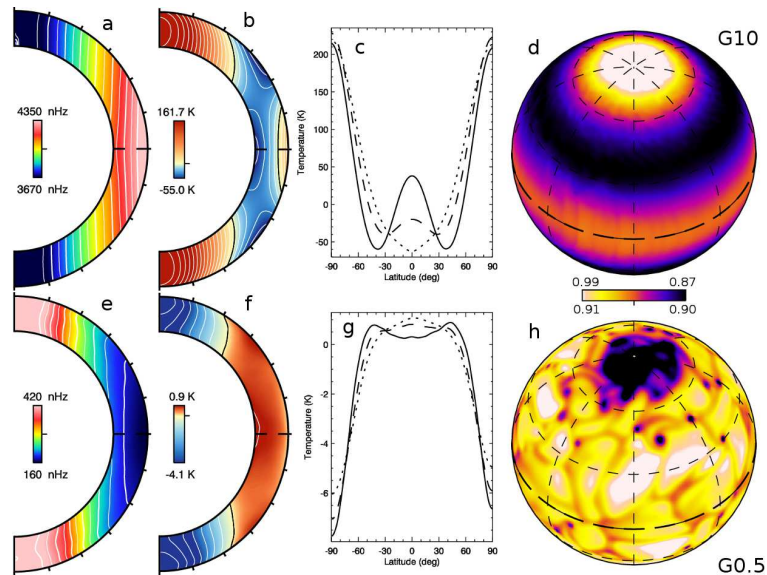


Figure 2. Global-scale signatures of convection. (a) Angular velocity of differential rotation in rapidly-rotating case G10. The flow is solar-like, with a fast equator and slower flows at the poles. The pole to equator contrast is about 10% near the surface. This zonal flow is substantially in thermal wind balance and the resulting temperature profile is shown in (b) with cuts at constant radius shown in (c) (solid near surface, dashed mid-convection zone, dotted bottom of convection zone). (d) Blackbody estimate of change in flux between polar and equatorial regions at the stellar photosphere, with hot north pole visible. Scale is relative to stellar average flux and is clipped. In slowly rotating stars like case G0.5, the sense of differential rotation may be anti solar (e) with fast poles and slower equator. The resulting thermal wind balance is cold at the poles and warm at the equator (f, g) which may result in dark poles (h) due to thermal effects rather than surface magnetism. Here the surface flux difference is a few percent.

into localized structures which may share many similarities with active longitudes of stellar magnetism.

In all solar-like stars the coupling of rotation with convection builds global-scale flows of differential rotation and meridional circulation. The profile of differential rotation is shown for case G10 in Figure 2a. In the Sun and in more rapidly rotating solar-type stars the angular velocity of differential rotation is faster near the equator and slower near the polar regions. Thus the equator rotates prograde relative to the poles, here with a relative contrast of about 10% between the equator and high-latitudes ( $\pm 60^\circ$ ). In contrast, the meridional circulations are quite weak in these stars, decrease in amplitude with faster rotation, and are generally multi-cellular in both radius and latitude (Brown et al. 2008).

The differential rotation is generally in a thermal-wind balance, and this results in a latitudinal temperature structure that is hot near the polar regions and cooler at mid-latitudes. In the Sun the magnitude of this contrast is probably only a few Kelvin and detecting this signature has been very challenging (e.g., Rast et al. 2008). In more

rapidly rotating stars the contrast may be much larger: here in case G10 a contrast of a few hundred Kelvin appears in the bulk of the convection zone and likely prints through to the stellar surface (Fig. 2*b,c*). A very simplistic blackbody flux estimate indicates that this may cause 10% or larger differences in the surface flux between the polar regions and the cooler mid-latitudes (Fig. 2*d*). More details on thermal-wind balance in simulations of solar-type stars can be found in Brun & Toomre (2002), Miesch (2005), Miesch et al. (2006, 2008), Ballot et al. (2007), and Brown et al. (2008).

At slower rotation rates the dynamics may be substantially different than in the rapidly rotating suns. In particular, as the rotational constraint weakens, the sense of differential rotation can flip and become anti-solar, with fast poles and a slow equator. This is shown for case G0.5 in Figure 2*e*, where the poles rotate nearly three times faster than the equator. These slowly spinning suns can remain in approximate thermal wind balance as well, though again the sense flips, now with cool poles and warm equators (Fig. 2*f,g*).

A striking consequence of this is that the poles may be relatively dark regions, due to fluid dynamic effects and irrespective of surface magnetic structures there. Here, under a simplistic blackbody flux approximation, the pole is a few percent dimmer than the warmer equator (Fig 2*h*). Polar spots on slowly rotating stars should be carefully examined to see whether any are due to non-magnetic effects. We note briefly that the designation “slowly spinning” is dependent on spectral type, and brighter, luminous F-type stars will be in the “slow” regime (high Rossby number) even if they rotate several times faster than our Sun currently does (Augustson et al. 2011). Conversely, less-luminous K- and M-type stars are likely “rapid rotators” (low Rossby numbers) even when spinning more slowly than the Sun. Dynamo solutions exist for the slowly spinning suns and these retain an anti-solar differential rotation, though again of reduced amplitude relative to the hydrodynamic simulations.

#### 4. Signatures of internal dynamics

The scaling of differential rotation and thermal-wind for the rapidly rotating simulations are shown in Figure 3. Generally, we find that the angular velocity shear between equator and high latitudes  $\Delta\Omega$  grows with faster rotation, though not as quickly as the rotation rate itself (a power-law of  $\Delta\Omega \propto \Omega^{0.3}$  is overplotted on cases rotating faster than  $3\Omega_{\odot}$ ). Owing to this, the relative angular velocity contrast

$$\Delta\Omega/\Omega = (\Omega(\text{equator}) - \Omega(\text{pole}))/\Omega(\text{equator}) \quad (1)$$

decreases as the rotation rate increases, here scaling as  $\Omega^{-0.6}$  (Brown et al. 2008). When magnetic fields are included and dynamo simulations are conducted, the global-scale magnetic fields weaken the large scale differential rotation (Fig. 3, asterisks). At present we are still sorting out how magnetism and differential rotation couple, and simulations right now are suggesting that the answer may change in different regimes of parameter space (e.g., cases D10 and D10L in Fig. 3*a*, and see Brown 2011).

The thermal-wind balance leads to progressively larger latitudinal contrasts of temperature in more rapidly rotating simulations (Fig. 3*b*). In the most rapidly rotating cases, the hot poles and the cool mid-latitudes can be nearly 300K different in temperature. If this latitudinal temperature gradient prints through the vigorous surface convection, then simple blackbody flux arguments would suggest that the poles could

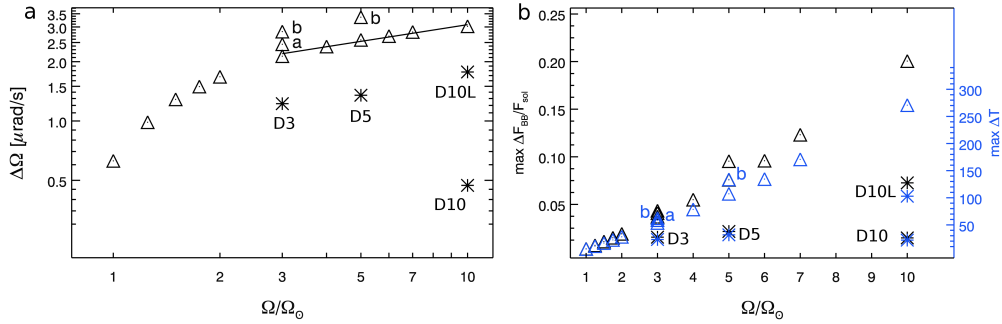


Figure 3. Signatures of differential rotation and the thermal wind (based on Brown et al. 2008). (a) Angular velocity shear of differential rotation  $\Delta\Omega$  in latitude near the stellar surface shown as a function of rotation rate  $\Omega$  relative to the solar rotation rate  $\Omega_\odot = 2.6\mu\text{rad/s}$ . Hydrodynamic cases are shown with diamonds while dynamos are labeled and shown with asterisks.  $\Delta\Omega$  grows with more rapid rotation in hydrodynamic cases. Cases labeled a and b sample more turbulent states. (b) Thermal-wind signatures. Shown in blue symbols (and right axis) are the largest latitudinal temperature contrasts achieved in these simulations. Shown in black symbols (and left axis) is the maximum of the relative blackbody flux contrast between the bright poles and dim mid-latitudes.

be up to 20% brighter than the cool mid-latitude bands (Fig. 3b, black symbols). The magnetic fields in the dynamo simulations reduce this signature as they reduce the differential rotation, and in those simulations the signature is about 5–10%. These blackbody fluxes are far too simple and neglect nearly all aspects of the stellar atmosphere, including viewing angle, but provide an order of magnitude initial estimate.

## 5. Wreath-building dynamos

The magnetic fields produced in these dynamo simulations may also have observational consequences. Generally, these rapidly rotating suns generate strong magnetic fields in the bulk of their convection zones. This is surprising as many solar dynamo theories hold that such organized dynamo action can only occur in the tachocline of shear and penetration located between the base of the convection zone and the stable radiative zone below. These simulations do not include that interface layer yet they still build organized fields.

Magnetic fields from two of the rapidly rotating dynamo cases are shown in Figure 4. These magnetic fields are organized in global-scale wreath-like structures, with complex topologies. Magnetic cycles are achieved in many of these dynamo simulations, including both cases D5 and D10L shown here. In some cases (e.g. D5 in Fig. 4a) the wreaths are highly axisymmetric and have opposite polarities in each hemisphere. During the magnetic cycle, wreaths of opposite polarity form in each hemisphere and at a later time the polarities will have reversed. Roughly 1500 days later the cycle repeats and returns the magnetic fields to a state like is shown here. In some cases (e.g. D10L in Fig. 4b) the wreaths may be much more concentrated in one hemisphere (here the southern). This simulation shows cycles of activity and in each successive cycle the



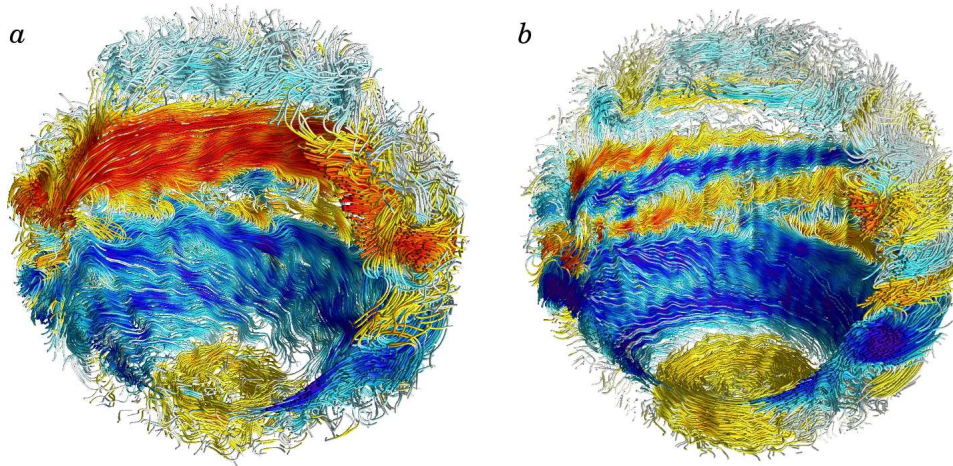


Figure 4. Magnetic wreaths in stellar convection zones. (a) Magnetic wreaths in cyclic case D5. Two wreaths of opposite polarity (red, positive; blue, negative) form above and below the equator. In this simulation the wreaths undergo reversals of polarity on roughly a 1500-day timescale. Relic wreaths from the previous cycle are visible in the polar caps. (b) Wreaths in more-rapidly rotating case D10L. Here a negative polarity axisymmetric wreath dominates the southern hemisphere while the northern hemisphere is filled with non-axisymmetric fields. During the next cycle the roles reverse and the wreath instead appears in the northern hemisphere, with tangled fields in the southern. Rings of relic fields are strongly evident at the southern pole. In both images the colortable saturates at  $\pm 25\text{kG}$ , while the fields may reach peak amplitudes of more than  $\pm 50\text{kG}$ .

wreaths alternate between the northern and southern hemisphere, though they rarely fill both at the same time. Magnetic fields are present in the other hemisphere (here the northern) but are less axisymmetric. In both case D5 and D10L there are significant rings of opposite polarity field located at the polar caps. These are relic fields from the preceding activity cycle (Brown et al. 2011).

## 6. Constraining simulations with interferometric observations

Modern simulations of convection in solar-type stars are able to self-consistently generate global-scale flows of differential rotation and meridional circulation. In the simulations, the convection and differential rotation drive strong dynamo action in the bulk of the stellar convection zone, generating coherent global-scale wreaths of magnetism. The zonal flow of differential rotation is likely the most easily observable signature of dynamics occurring deep within the stellar interior. Its characterization is thus of crucial importance. Despite this, current observations are in significant disagreement (e.g., Donahue et al. 1996; Barnes et al. 2005), and there are hints of very interesting relationships between  $\Delta\Omega$  and the X-ray luminosity of stars (Saar 2009).

Simulations predict that the angular velocity contrast in latitude should grow larger in solar-type stars as they rotate more rapidly. At the highest rotation rates, the relative contrast  $\Delta\Omega/\Omega \sim 10\%$ , which at ten times the solar rotation rate (case G10, with

Table 1. A few possible observational targets

Name	HD	Spectral type	parallax	Vmag	Vrot	$R/R_{\odot}$	$\Omega/\Omega_{\odot}$
tet Boo	126660	F7V	68	4.1	32	1.5	10
chi Dra	170153	F7V	124	3.6	8	1.1	4
86 Her	161797	G5IV	119	3.4	8	1.5	3
GJ 702 A	165341A	K0V	196	4.2	16	0.8	10

rotation period of about 3 days) would lead to an equatorial velocity of about 20 km/s and a high-latitude ( $60^{\circ}$  latitude) velocity of about 14 km/s (versus 17 km/s for solid body rotation). These are clearly challenging observations but may lie within reach for current interferometers (e.g., VEGA at CHARA). To inspire such searches, a few of the nearby, rapidly-rotating and bright solar-type stars which should be accessible to northern-hemisphere interferometers are listed in Table 1. Rotation rates here are lower limits, based on  $V_{\text{ sini}}$  from SIMBAD and rough estimates of stellar radii from Pasinetti Fracassini et al. (2001).

The differential rotation may be in thermal wind balance and this may lead to latitudinal gradients of temperature. These may in turn lead to gradients of the stellar flux equal to a few percent in brightness. Solar-like differential rotation is probably accompanied by relatively warm poles and cool mid-latitudes, while anti-solar differential rotation would have cool poles and warm equators. These thermal signatures are non-magnetic in nature.

Lastly, the global-scale longitudinal and radial magnetic fields associated with these wreaths may appear at or near the stellar surface. Observations with Zeeman-Doppler Imaging (ZDI) techniques appear to show evidence for large-scale longitudinal magnetic fields at or near the stellar surfaces (e.g., Petit et al. 2008; Marsden et al. 2011). Interferometric spectroscopic observations may be able to spatially resolve these structures, providing critical tests for both the simulations and the growing field of ZDI observations, which can in principle be applied to more distant objects. Characterizing the large-scale poloidal field may also provide indirect indications of large wreaths lurking beneath the stellar photospheres.

**Acknowledgments.** This research on wreath-building dynamos in solar-type stars has been done in collaboration with Kyle C. Augustson, Matthew K. Browning, Allan Sacha Brun, Mark S. Miesch, Nicholas J. Nelson and Juri Toomre, and I owe them many thanks. Funding for this research is provided in part through NSF Astronomy and Astrophysics Postdoctoral Fellowship AST 09-02004. CMSO is supported by NSF grant PHY 08-21899. The simulations were carried out with NSF PACI support of NICS, PSC and TACC. Field line tracings shown in Figure 4 were produced using VAPOR (Clyne et al. 2007). This research has made use of the SIMBAD database, operated at CDS, Strasbourg, France



**References**

- Augustson, K., Brown, B. P., Brun, A. S., & Toomre, J. 2011, ApJ, in preparation
- Ballot, J., Brun, A. S., & Turck-Chièze, S. 2007, ApJ, 669, 1190. arXiv:0707.3943
- Barnes, J. R., Cameron, A. C., Donati, J.-F., James, D. J., Marsden, S. C., & Petit, P. 2005, MNRAS, 357, L1. arXiv:astro-ph/0410575
- Brown, B. 2011, Journal of Physics Conference Series, 271, 012064. 10.1088/1742-6596/271/1/012064
- Brown, B. P., Browning, M. K., Brun, A. S., Miesch, M. S., & Toomre, J. 2008, ApJ, 689, 1354. 0808.1716
- 2010, ApJ, 711, 424. 10.1088/0004-637X/711/2/424
- Brown, B. P., Miesch, M. S., Browning, M. K., Brun, A. S., & Toomre, J. 2011, ApJ, 731, 69:1. 1102.1993
- Browning, M. K., Miesch, M. S., Brun, A. S., & Toomre, J. 2006, ApJ, 648, L157. arXiv:astro-ph/0609153
- Brun, A. S., Miesch, M. S., & Toomre, J. 2004, ApJ, 614, 1073
- Brun, A. S., & Toomre, J. 2002, ApJ, 570, 865. arXiv:astro-ph/0206196
- Clune, T. L., Elliott, J. R., Glatzmaier, G. A., Miesch, M. S., & Toomre, J. 1999, Parallel Computing, 25, 361
- Clyne, J., Mininni, P., Norton, A., & Rast, M. 2007, New Journal of Physics, 9, 301
- Donahue, R. A., Saar, S. H., & Baliunas, S. L. 1996, ApJ, 466, 384
- Ghizaru, M., Charbonneau, P., & Smolarkiewicz, P. K. 2010, ApJ, 715, L133
- Marsden, S. C., Jardine, M. M., Ramírez Vélez, J. C., Alecian, E., Brown, C. J., Carter, B. D., Donati, J.-F., Dunstone, N., Hart, R., Semel, M., & Waite, I. A. 2011, MNRAS, 413, 1922. 1101.5859
- Miesch, M. S. 2005, Living Reviews in Solar Physics, 2, 1:1
- Miesch, M. S., Brun, A. S., DeRosa, M. L., & Toomre, J. 2008, ApJ, 673, 557. arXiv:0707.1460
- Miesch, M. S., Brun, A. S., & Toomre, J. 2006, ApJ, 641, 618
- Miesch, M. S., & Toomre, J. 2009, Annual Review of Fluid Mechanics, 41, 317
- Pasinetti Fracassini, L. E., Pastori, L., Covino, S., & Pozzi, A. 2001, A&A, 367, 521. arXiv:astro-ph/0012289
- Petit, P., Dintrans, B., Solanki, S. K., Donati, J.-F., Aurière, M., Lignières, F., Morin, J., Paletou, F., Ramirez Velez, J., Catala, C., & Fares, R. 2008, MNRAS, 388, 80. 0804.1290
- Pizzolato, N., Maggio, A., Micela, G., Sciortino, S., & Ventura, P. 2003, A&A, 397, 147
- Racine, É., Charbonneau, P., Ghizaru, M., Bouchat, A., & Smolarkiewicz, P. K. 2011, ApJ, 735, 46
- Rast, M. P., Ortiz, A., & Meisner, R. W. 2008, ApJ, 673, 1209. 0710.3121
- Saar, S. H. 2009, in Solar-Stellar Dynamos as Revealed by Helio- and Asteroseismology: GONG 2008/SOHO 21, edited by M. Dikpati, T. Arentoft, I. González Hernández, C. Lindsey, & F. Hill, vol. 416 of Astronomical Society of the Pacific Conference Series, 375